

Marine Boundary Layer Cloud Observations in the Azores

JASMINE RÉMILLARD AND PAVLOS KOLLIAS

Department of Atmospheric and Oceanic Sciences, McGill University, Montreal, Quebec, Canada

EDWARD LUKE

Atmospheric Sciences Division, Brookhaven National Laboratory, Upton, New York

ROBERT WOOD

Department of Atmospheric Sciences, University of Washington, Seattle, Washington

(Manuscript received 19 October 2011, in final form 12 April 2012)

ABSTRACT

The recent deployment of the Atmospheric Radiation Measurement Program (ARM) Mobile Facility at Graciosa Island, Azores, in the context of the Clouds, Aerosol and Precipitation in the Marine Boundary Layer (CAP-MBL) field campaign added the most extensive (19 months) and comprehensive dataset of marine boundary layer (MBL) clouds to date. Cloud occurrence is high (60%–80%), with a summertime minimum. Liquid precipitation is frequently present (30%–40%), mainly in the form of virga. Boundary layer clouds are the most frequently observed cloud type (40%–50%) with a maximum of occurrence during the summer and fall months under the presence of anticyclonic conditions. Cumulus clouds are the most frequently occurring MBL cloud type (20%) with cumulus under stratocumulus layers (10%–30%) and single-layer stratocumulus (0%–10%) following in frequency of occurrence. A stable transition layer in the subcloud layer is commonly observed (92% of the soundings). Cumulus cloud bases and stratocumulus cloud tops correlate very well with the top of the transition layer and the inversion base, respectively. Drizzling stratocumulus layers are thicker (350–400 m) and have higher liquid water path (75–150 g m⁻²) than their nondrizzling counterparts (100–250 m and 30–75 g m⁻², respectively). The variance of the vertical air motion is maximum near the cloud base and is higher at night. The updraft mass flux is around 0.17 kg m⁻² s⁻¹ with 40%–60% explained by coherent updraft structures. Despite a high frequency of stratocumulus clouds in the Azores, the MBL is almost never well mixed and is often cumulus coupled.

1. Introduction

Marine stratocumulus clouds are ubiquitous over the eastern subtropical oceans and play a critical role in the boundary layer dynamics and the global climate (e.g., Klein and Hartmann 1993; Bony and Dufresne 2005). These prevailing low-level cloud decks are a key component in the earth's radiation budget (Randall et al. 1984; Ramanathan et al. 1989). The radiative impact of marine boundary layer clouds depends on their macroscopic properties (e.g., horizontal extent, thickness) and microscopic properties (e.g., particle size distribution).

Past studies have focused on the cloud macrostructure properties of marine boundary layer clouds and their relationship to large-scale dynamics and thermodynamic state using satellite observations and reanalysis products (e.g., Klein and Hartmann 1993; de Szoeke and Xie 2008). Wood and Bretherton (2006) have shown that approximately 80% of the variance in low cloud cover in regions dominated by marine stratocumulus is explained using the estimated inversion strength. However, appreciable complexity and challenges are found on smaller space and time scales, including the cloud microscale (spatial scales of tens of meters and temporal scales of a few minutes or less).

Previous field experiments focusing on marine stratocumulus clouds include the Atlantic Stratocumulus Transition Experiment (ASTEX) (Albrecht et al. 1995), the East Pacific Investigation of Climate (EPIC)

Corresponding author address: Jasmine Rémillard, Department of Atmospheric and Oceanic Sciences, Room 945, Burnside Hall, 805 Sherbrooke Street West, Montreal QC H3A 2K6, Canada.
E-mail: jasmine.remillard@mail.mcgill.ca

(Bretherton et al. 2004), the Dynamics and Chemistry of Marine Stratocumulus (DYCOMS) (Stevens et al. 2003), and the Variability of the American Monsoon Systems (VAMOS) Ocean–Cloud–Atmosphere–Land Study Regional Experiment (VOCALS-REx) (Wood et al. 2011). These field studies advanced our knowledge of marine stratocumulus, providing information on their boundary layer thermodynamic and cloud structure, as well as their diurnal cycle. They have highlighted that stratocumulus clouds can form under a diverse range of conditions, in both deep and shallow marine boundary layers (MBL), and under a wide range of aerosol conditions. Furthermore, the radiative properties and propensity for drizzle from marine stratocumulus clouds depend on several factors including aerosols, liquid water path, and dynamics.

The aforementioned field campaigns are characterized by intensive observation periods limited in time from a couple of weeks to a month. Thus, previous studies have not been carried out long enough to provide a useful climatology of key MBL and associated cloud properties. The recent Clouds, Aerosol and Precipitation in the Marine Boundary Layer (CAP-MBL) field campaign (<http://www.arm.gov/sites/amf/grw/>), which took place in the Azores, nicely filled that gap. As part of the campaign, the U.S. Department of Energy Atmospheric Radiation Measurement Program (ARM) Mobile Facility (AMF) was deployed on Graciosa Island. This AMF deployment is unique compared to previous intensive field campaigns. First, the AMF instrumentation is far more comprehensive and superior to that available in previous ground-based field studies. Second, the campaign is 21 months long and thus provides the opportunity to generate the long dataset record required to sample a variety of aerosol, cloud, and large-scale environmental conditions. Finally, it is the first marine stratocumulus field campaign with sophisticated cloud radars (profiling and scanning) on a stable (island) platform that enables the use of the Doppler velocity measurements. Thus, the AMF deployment in the Azores produced the most comprehensive dataset of MBL clouds to date.

In this study, we select a subset of the deployed AMF instruments to study the observed MBL clouds in more detail. An objective scheme was first developed to identify their occurrence across the entire dataset and to recognize some important subtypes (e.g., cumulus and stratocumulus), with the presence of precipitation also diagnosed (see section 3). The variability and frequency of occurrence of the different cloud and precipitation events is presented with emphasis on the various MBL cloud structures. A further analysis of the MBL emphasizes the differentiation between cumulus and stratocumulus regimes as well as the presence of decoupling. A statistical analysis of cloud structural and dynamical

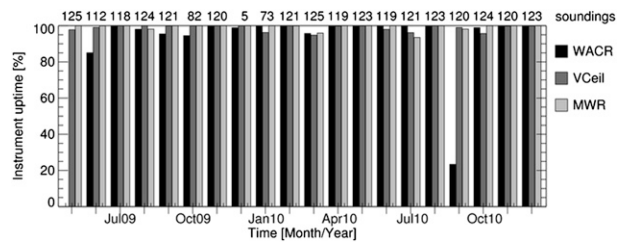


FIG. 1. Monthly statistics of good running time for the WACR (black), ceilometer (dark gray), and MWR (light gray). Operations are considered bad when more than a minute separates successive measurements. Note that the radar started working in early June 2009, and it was down for about 23 days in September 2010. Note also that the radiometer measurements from 11 Jul through 9 Aug 2010 are unreliable, owing to a software problem, although it is not shown here. The numbers above the graph represent the number of soundings taken during each month that returned good measurements.

properties is performed and related to the thermodynamic profiles.

2. Observations

The CAP-MBL field campaign lasted 21 months (April 2009–December 2010), permitting the sampling of almost two full years of cloud and precipitation conditions in the Azores. Although this location has been used in the past for the study of marine stratocumulus clouds (ASTEX), a variety of cloud conditions were sampled that include shallow cumulus, cumulus under stratocumulus, deeper convection, and frontal systems. The AMF—with its usual comprehensive array of aerosol, cloud, precipitation, and radiation sensors—was deployed near the north shore of Graciosa Island (39.09°N, 28.03°W, 26 m MSL). This location is upwind for the climatologically prevailing wind conditions in the MBL and was selected to reduce the island effect. The primary instruments used in this study to describe the cloud and precipitation conditions are 1) a W-band (95-GHz) Doppler radar, 2) a laser ceilometer, 3) a two-channel microwave radiometer (MWR), and 4) radiosondes (four per day). The instruments were placed within a few meters of each other; thus, to the extent possible, their measurements describe the same atmospheric column. The operational status of the three remote sensors is summarized in Fig. 1, allowing gaps of up to one minute to be considered within normal operation. Overall, the observations are fairly continuous with great overlap between the three remote sensors, spatially as well as temporally.

a. W-band Doppler radar

A baseline instrument of the AMF is the W-band ARM Cloud Radar (WACR) (Mead and Widener 2005), a

95-GHz vertically pointing Doppler radar. Millimeter-wavelength radars are ideally suited for the study of MBL clouds (e.g., Kollias et al. 2007a). Owing to its short wavelength (3.15 mm), it is sensitive enough to detect cloud droplets (-50 dBZ at 2 km), while attenuation is small in light to moderate drizzle conditions. Furthermore, it uses a beamwidth narrow enough (0.19°) to provide high temporal and spatial resolutions (around 2 s and 43 m). Its primary measurement is the Doppler spectrum, reporting the full distribution of the returned radar echo over the range of sampled Doppler velocities (here ± 7.885 m s $^{-1}$ with a resolution near 6 cm s $^{-1}$). Thus, detailed information about cloud microphysics and dynamics is inherent in the radar measurements (e.g., Kollias et al. 2011a; Luke et al. 2010). The WACR also provides an estimate of hydrometeor (i.e., cloud and drizzle) boundaries (see section 3a below), as it is only sensitive to these atmospheric particles. However, some parts of nonprecipitating liquid clouds might be missed if the cloud droplets are not large enough, and heavy precipitation strongly attenuates the signal affecting the cloud top measurements. For the Azores deployment, the WACR began operating on the morning of 5 June 2009 and operated until the end of the campaign. One major interruption occurred in September 2010, when the radar was down for almost 23 days, due to a hard disk problem. Otherwise, the radar experienced six downtimes of more than an hour (including three extending over about 1.5 days) and a few shorter, for a total of less than 10% of a month (see Fig. 1, black bars). Note also that the radar used alternating copolarized (H-H) and cross-polarized (H-V) operating modes through late 2009, after which it operated continuously in copolarized mode. The cross-polarized measurements are not used here since MBL clouds have spherical cloud and drizzle particles. Therefore, the time between profiles is around 4 s for the earlier months and 2 s for the latter. Nonetheless, given the horizontal scales of the sampled clouds the results should not be affected by that change.

b. Ceilometer

Another baseline AMF instrument is a Vaisala ceilometer (CT25K model, upgraded in mid July 2010 to the CL31 model; M \ddot{u} nk \ddot{u} l et al. 2007), a near-infrared vertically pointing lidar. It provides profiles of the atmospheric column, sensing aerosols and hydrometeors mainly up to the liquid cloud base, as cloud droplets prevent in-cloud measurements by extinguishing the laser signal. Nevertheless, the sharp increase and subsequent decrease of the lidar backscatter at the level of the cloud base is very useful for deriving the actual cloud base height, while still being able to profile drizzle and aerosols particles under the cloud (e.g., O'Connor et al.

2005; Markowicz et al. 2008). Although up to three liquid layer bases are reported in the ceilometer products, usually only the first one is reliable. This is due to the quick depletion of the lidar signal strength by the numerous cloud droplets, and it depends on the amount of liquid encountered in lower cloud layers. The ceilometer's temporal resolution was around 15 s for this deployment, which is slightly coarser than for the WACR. Here, it is assumed that each reported base height is representative of the whole 15 s. The ceilometer range resolution is 15 m. Thus, the analysis is done using the original WACR temporal grid, maintaining the high sampling rate of the WACR. The ceilometer was deployed for the whole duration of the campaign. It only experienced 12 downtimes lasting more than an hour (including three covering more than a day), as well as a small number of shorter interruptions (see the dark bars in Fig. 1).

c. Microwave radiometer

A standard Radiometrics two-channel microwave radiometer (MWR) was also present throughout the campaign. This instrument passively measures the amount of radiation emitted by the atmosphere at two frequencies (23.8 and 31.4 GHz) to retrieve the amount of integrated water in the atmospheric column overhead, separated into the vapor and liquid phases [the precipitable water vapor (PWV) and liquid water path (LWP); e.g., Liljegren 1994]. Such information can help constrain retrievals from other instruments, such as the WACR. The MWR time resolution is around 30 s, which is also coarser than for the WACR. Nevertheless, as the MWR measurements actually come from 20-s signal dwells, it is reasonable to consider each retrieved quantity to be representative of the whole 30 s. Therefore, these measurements are oversampled to match the high temporal resolution of the WACR when required by the analysis. The root-mean-square accuracy of the LWP retrieval is around 20–25 g m $^{-2}$. As with the ceilometer, the MWR was deployed for the whole campaign and it worked continuously without much interruption of data (see Fig. 1, light bars). However, the MWR experienced a processing problem in the second summer, rendering the measurements reported from 11 July through 9 August 2010 unreliable (not shown in Fig. 1 as measurements are available regardless). Note also that the presence of water on the instrument's window contaminates the measurements, rendering its retrievals unreliable. This happens anytime precipitation reaches the ground.

d. Radiosondes

Regular radiosonde launches (every 6 h) were performed throughout the deployment to characterize the

thermodynamic state of the atmosphere as well as the wind speed and direction. The radiosondes collect measurements every 2 s during their ascent, providing a typical vertical resolution of 10 m in the troposphere (depending on the conditions at the launch time). These measurements can only be interpolated to the WACR time steps with limited confidence, owing to the coarse temporal resolution of the radiosondes. However, some statistics can still be determined around the balloon launch times since there are 20 months of data comprising more than 2200 atmospheric profiles, although no sondes were launched in the last third of October 2009 or from 2 December 2009 through 12 January 2010 (see the numbers at the top of Fig. 1).

3. Methodology

All instruments described in the previous section have certain skill for detecting the presence of clouds in the overlying atmospheric column. For instance, relative humidity profiles taken by a radiosonde have been used in the past to provide estimates of cloud layer locations (e.g., Wang and Rossow 1995). However, their temporal resolution is too coarse to form robust statistics of cloud occurrence, especially in the MBL, where clouds are typically very thin. The MWR is sensitive to the presence of liquid in the column, and measurements above its theoretical sensitivity ($30\text{--}50\text{ g m}^{-2}$) can be used to infer the occurrence of liquid clouds. However, the MWR misses all ice clouds (mostly cirrus clouds in the Azores), as their thermal emission is negligible at the frequencies sensed by the MWR (Ulaby et al. 1981). Similarly, the ceilometer measurements are very sensitive to the presence of cloud droplets, providing a good estimate of the base height of liquid clouds; its backscatter profiles can be used to find ice cloud too (e.g., Liu et al. 2009). Nevertheless, it still misses most high clouds, as its useful range stops near 7.5 km. Finally, the WACR is sensitive to most hydrometeors and profiles all clouds in the troposphere, unless strong precipitation occurs and causes too much attenuation (Lhermitte 1990). However, it cannot easily differentiate precipitation from cloud particles (so cannot be used to reliably provide cloud base estimates in drizzling conditions) and lacks sensitivity to very thin liquid clouds (less than 100 m thick).

Here, a multi-instrument approach that utilizes synergistic measurements from all sensors is used to describe the cloud and precipitation conditions during CAP-MBL. Because of the focus on describing the vertical structure of clouds and precipitation, only the active remote sensor (radar and lidar) measurements are used for the cloud and precipitation occurrence statistics, while the MWR and the soundings are used as

additional classification variables. The approach is not new: the cloud radar and lidar are complementary instruments often used to derive cloud and precipitation statistics (e.g., Intrieri et al. 2002; Bretherton et al. 2004; Kollias et al. 2007b; Illingworth et al. 2007).

Using the raw WACR measurements [radar reflectivity and signal-to-noise ratio (SNR)] the radar range gates that contain significant returns from atmospheric targets (e.g., hydrometeors) are identified to develop the radar-detected hydrometeor mask. The large number of WACR integrated radar pulses ($\sim 20\,000$ collected in 2-s signal dwell and a WACR pulse repetition frequency of 10 kHz) enables it to detect very low signal to noise radar returns in the boundary layer (WACR sensitivity of -56 dBZ at 1 km). The significant detection WACR hydrometeor mask is based on Clothiaux et al. (1995), and a two-dimensional (time–height) filter is used to remove isolated radar pixels. The WACR-derived hydrometeor mask is used to estimate the number of hydrometeor layers in the atmospheric column and their corresponding boundaries. The WACR-derived hydrometeor layer base is not necessarily the cloud base since the WACR cannot differentiate between cloud and precipitation particles below the cloud base. Thus, the radar-derived hydrometeor mask is combined with the ceilometer-generated time series of cloud-base heights. Although the ceilometer detects drizzle too, its measurements are more sensitive to the numerous small liquid cloud droplets encountered by the laser at the cloud base and thus are systematically used to derive the liquid cloud base, at least for the first cloud layer. As formerly observed (e.g., Comstock et al. 2004; Wood et al. 2011), heavy drizzle often gives false signals, by significantly lowering the ceilometer-derived cloud-base height. During heavy precipitation, the cloud identification will still be reliable, but further analysis of MBL clouds would be compromised. Thus, the profiles containing intense precipitation (defined below) are removed prior to subsequent analysis.

The WACR/ceilometer detections agree very well in the MBL; however, the possibility of underestimating the hydrometeor occurrence at high altitude should be considered since the ceilometer is not capable of detecting high clouds and the radar sensitivity is degraded. The WACR moments, the radar-derived hydrometeor mask, and the ceilometer-derived liquid cloud base are inputs to the cloud and precipitation type identification scheme described in the following section.

a. Cloud and precipitation type identification

A WACR echo is classified as precipitation if it is detected below the ceilometer cloud-base height. The first category of precipitation is virga, defined as

TABLE 1. List of liquid precipitation types and their main characteristics used to differentiate them.

	Type		
	Virga	Light	Intense
Echo base	>200 m	<200 m	<200 m
Base reflectivity	—	<0 dBZ	≥0 dBZ
Echo below cloud base	Yes	Yes	Possible

precipitation that does not reach the lowest WACR range gate (i.e., no significant radar return at its lowest range gate, around 170 m AGL; see Table 1). In cases where the WACR echoes reach the lowest range gate (here taken as a proxy for the surface) two more precipitation categories are identified: light and intense. The separation between these two precipitation types is based on a near-surface (200 m) radar reflectivity threshold of 0 dBZ. Anytime that the WACR lowest gate echoes have a reflectivity above 0 dBZ, intense precipitation is designated, regardless of the ceilometer cloud-base height since the ceilometer measurements are significantly affected by the presence of water on its lens cover. The use of a radar reflectivity threshold is justified given the absence of disdrometer measurements in the Azores. Furthermore, the MBL clouds produce drizzle echoes below 0 dBZ; thus, the intense category of precipitation is almost exclusively related to deeper cloud systems (e.g., frontal precipitation). The distinction between virga and light precipitation provides a qualitative indicator of the drizzle intensity and indicates the portion of the subcloud layer that was affected by evaporation.

Using the WACR-derived hydrometeor mask and the ceilometer-derived cloud bases, groups of connected pixels containing hydrometeors are identified. Each of these hydrometeor clusters is individually analyzed on an hourly basis, with the hydrometeor layer base (top) defined as the 5th (95th) percentile of the hourly distribution of the cloud cluster base (top). Based on their hourly derived base and top height extrema and the available ceilometer-derived cloud-base height, several cloud types are identified (columns in Table 2). The

hourly clusters are first separated into four types based specifically on these boundary definitions: 1) high cloud if the base is above 7 km; 2) middle cloud if the base is above 3 km; 3) low cloud if the top is below 3 km; and 4) deep boundary layer cloud if the base is below 3 km but the top is above 3 km. Note that the last category contains mostly frontal clouds, such as nimbostratus and cumulonimbus. Since the focus of this study is MBL clouds, emphasis is placed on low clouds, where the radar and lidar are most sensitive, allowing for well-defined cloud boundaries. As a result, low clouds are further divided into three subtypes: broken, stratocumulus, and indeterminate. The temporal duration of a hydrometeor cluster is used to differentiate broken cloud conditions (shallow cumulus) from stratiform cloud conditions, while stratocumulus are also required to have a narrow hourly cloud-top height distribution (less than 100-m standard deviation). Examples of stratiform and broken MBL cloud conditions as seen by the WACR and Moderate Resolution Imaging Spectroradiometer (MODIS) are shown in Fig. 2. The remaining low cloud hourly clusters make up the third subtype (referred to as indeterminate hereafter). Each cloud type has an expected precipitation type (last row of Table 2), although others are also possible. Note that the lidar measurements rarely reach high clouds, and thus no precipitation shaft is expected. Note also that the cloud types are not all mutually exclusive since clouds are observed only in time and height, yet they are also evolving in the two horizontal dimensions.

The cloud and precipitation identification scheme is applied each day when both the WACR and ceilometer were operational, and statistics about cloud and precipitation occurrences are computed on hourly and daily basis, with the daily results composited together to form monthly statistics. Note that the hourly derived boundaries extrema are only used to identify the cloud types. Further analysis makes use of the full distribution of the hourly cloud base and top heights to provide their statistics. Finally, the occurrences of cumulus clouds under a stratocumulus cover are investigated. These represent

TABLE 2. List of cloud types and their main characteristics used to differentiate them in the identification algorithm (Ind: indeterminate). The last row indicates the type of precipitation most likely associated with each cloud type.

Characteristic	Type					
	High	Middle	Low			Deep BL
			Cu	Sc	Ind	
Cloud base	>7 km	>3 km	—	—	—	≤3 km
Cloud top	—	—	≤3 km	≤3 km	≤3 km	>3 km
Duration	—	—	<20 min	≥20 min	≥20 min	—
CT variability	—	—	—	<100 m	≥100 m	—
Type of precipitation	—	Virga	Virga	Light	Intense	Intense

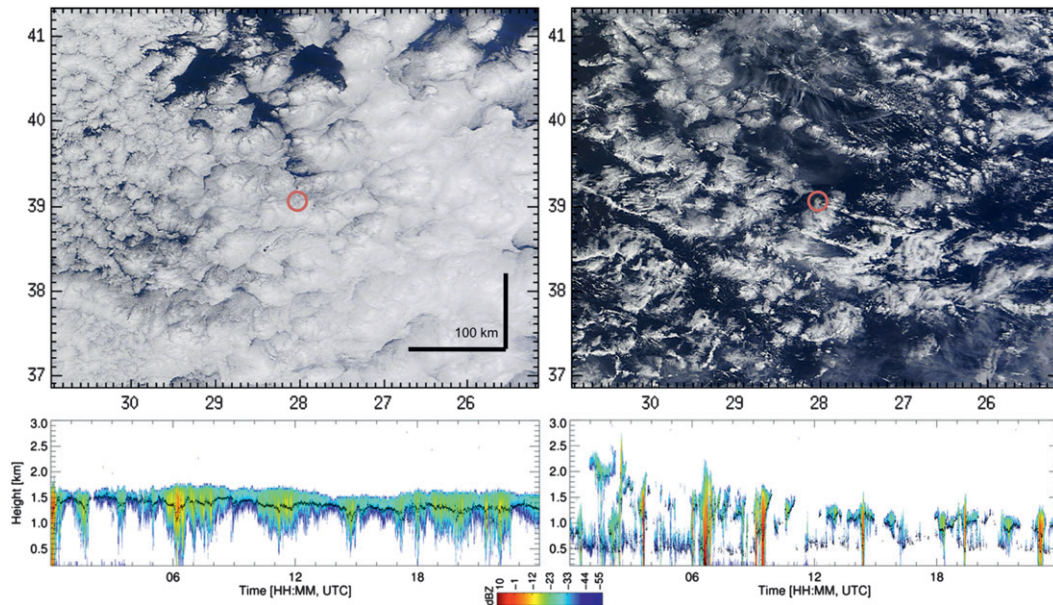


FIG. 2. (top) True color images from MODIS onboard *Terra* taken around 1315 UTC and spanning about 500 km in both dimensions centered at the location of Graciosa Island (shown in red circle). (left) A stratocumulus cloud case (22 Nov 2009) and (right) a broken cumulus (0300–0600 UTC) and cumulus with stratocumulus (1800–2400 UTC) cases (30 Aug 2010). (bottom) The corresponding daily WACR time–height reflectivity observations with the first ceilometer cloud base shown as black dots.

the WMO-defined low cloud type CL8 and are diagnosed on an hourly basis. When both types are detected in any number of profiles within an hour, all profiles having cumulus and/or stratocumulus clouds within that same hour are included in the Sc + Cu category.

b. Radiosonde analysis

Radiosonde data are not used directly in cloud identification but are used to determine the thermodynamic structure of the lower atmosphere during certain cloud conditions. For instance, the inversion often associated with the top of the MBL is easily detected in sounding profiles. A temperature increase with height somewhere between 500 m (to avoid surface effects) and 3 km (to remain in the MBL) denotes the presence of an inversion. The level of maximum increase indicates the inversion layer location and it includes all levels around it still characterized by an increase. Since wetting affects the temperature measurements above clouds (Caldwell et al. 2005), a loose criterion on the water vapor mixing ratio (r) was added by requiring its decrease with height.

Many studies have also mentioned the presence of a transition layer in the MBL, which separates a surface mixed layer from the cloud-containing layer aloft (Augstein et al. 1974; Garstang and Betts 1974; Yin and Albrecht 2000). It is mainly characterized by a sharp decrease of moisture with height, accompanied by a slight increase in

temperature. It indicates the presence of decoupling conditions that can lead to a cutoff of the upper part of the MBL from its moisture supply, thus controlling low-level cloudiness. Cumulus clouds often form near its top, as the surface lifting condensation level often falls within the transition layer (Yin and Albrecht 2000). Following Yin and Albrecht, the presence of a transition layer will be investigated using their parameter μ , which combines the potential temperature θ and mixing ratio r gradients with respect to the pressure p in the following way:

$$\mu = -\left(\frac{\partial\theta}{\partial p} - \frac{0.608\theta}{1 + 0.608r} \frac{\partial r}{\partial p}\right).$$

Its mean value is computed using all levels below the inversion. Then, if the maximum value of μ in those levels is positive and greater than 1.3 times the mean (based on Yin and Albrecht 2000), a transition layer is present. The transition layer includes all levels around the μ maximum that satisfy this criterion.

As the detection of these two layers depends on the derivative of the measured variables, a 1–2–1 smoother is applied prior to any analysis. This step removes most of the small-scale variability that might be caused by sampling errors (although the data were already smoothed by the radiosonde software itself) and provides smooth local gradients. Also, when averaging various profiles together,

a layer-by-layer procedure is used to preserve the character of the transition and inversion layers [based on Augstein et al. (1974) and Yin and Albrecht (2000)]. For each sounding, five layers are defined: below the transition base, the transition layer, from the transition top to the inversion base, the inversion layer, and above the inversion top (up to 3 km). Each layer is averaged separately using a relative height coordinate (from 0 to 1). The averaged sounding is then obtained by combining the five resulting averaged layers, using the averaged base and top heights of the layers to get the height coordinate.

The lower-tropospheric stability (LTS) is also used in this study. Based on Klein and Hartmann (1993), it is defined as the difference in potential temperature between 700 mb and the surface. Finally, any interpolated (or averaged) wind direction is obtained from the two interpolated (or averaged) components of the wind vector.

c. Turbulence and mass flux measurements

During nonprecipitating cloud conditions, the WACR Doppler velocity measurements are used to derive turbulence statistics in low-level stratiform cloud conditions. This is based on the assumption that liquid cloud particles have negligible terminal velocity and inertia and, thus, act as tracers of the vertical air motion (e.g., Kollias et al. 2001). Only stratocumulus periods without drizzle detected under the ceilometer base are considered in these statistics, in order to remove most bias caused by the larger precipitating particles. The WACR Doppler velocity measurements are used to estimate the hourly estimates of the mean, variance, and skewness of the vertical air motion. Using the vertical air motion measurements, mass flux statistics are also estimated during nonprecipitating stratocumulus conditions to reduce any correlations between drop fall velocities and WACR Doppler measurements. Although Kollias et al. (2011b) showed that drizzle drops are ubiquitous in marine stratocumulus clouds, their impact on the velocity moments remains negligible in nondrizzling parts.

Using the high-resolution in-cloud vertical velocity measurements, the mass flux profiles are derived using two conditional sampling strategies (based on Kollias and Albrecht 2000). They are both based on the WACR perturbed velocities, which are obtained by removing the hourly mean from the velocity measurements. The first method (a classic direct sampling) simply uses the sign of these perturbed velocities to determine the presence of updraft and downdraft regions. The second method (the coherent sampling) refines this by using the cloud coherent structures only. Those structures are pockets of clouds that move together on average. Coherent structures must be observed in both dimensions: the perturbed vertical velocity must conserve its sign for three or more successive

profiles (time dimension, which relates to the horizontal dimension) and over at least four successive gates (i.e., about 170 m in the vertical dimension). Both methods directly retrieve the fractional updraft area (σ) and the updraft and downdraft velocities (w_u and w_d), with the second one providing the contribution from the coherent structures. The convective mass flux (M_c) can then be computed from the following: $M_c = \rho\sigma(1 - \sigma)(w_u - w_d)$, where ρ is the air density.

The mass flux profiles are also computed using the turbulence statistics as proposed by Randall et al. (1992). This method relates σ and M_c to turbulence statistics. It uses a “top hat” representation of the updrafts and downdrafts properties to express σ , w_u , and w_d as functions of the first three moments of the vertical velocity (mean \bar{w} , variance w'^2 , and skewness S_w):

$$\sigma = \frac{1}{2} - \frac{S_w}{2\sqrt{4 + S_w^2}},$$

$$w_u = \bar{w} + \frac{\sqrt{w'^2}}{2} (\sqrt{4 + S_w^2} + S_w),$$

$$w_d = \bar{w} - \frac{\sqrt{w'^2}}{2} (\sqrt{4 + S_w^2} - S_w).$$

Then, the relationship for the convective mass flux depends only on the variance and skewness of the vertical velocity:

$$M_c = \frac{\rho\sqrt{w'^2}}{\sqrt{4 + S_w^2}},$$

[for the complete derivation of the equations, see Randall et al. (1992)]. In the following results, the mass flux values are normalized by ρ . The application of the Randall et al. approach to estimate the fractional area of the updrafts and the updraft mass flux and its comparison with the direct and coherent methods are used as a qualitative indicator of how close to the top-hat representation of updrafts and downdrafts the observed vertical air motion is. Furthermore, it is an indicator of how well high-order closure models can be used to determine the area and mass flux of updrafts.

4. Results

a. Cloud and liquid precipitation occurrence

Using the radar–lidar synergistic observations, the monthly fraction of time hydrometeors detected in the atmospheric column is shown in Fig. 3a. A weak

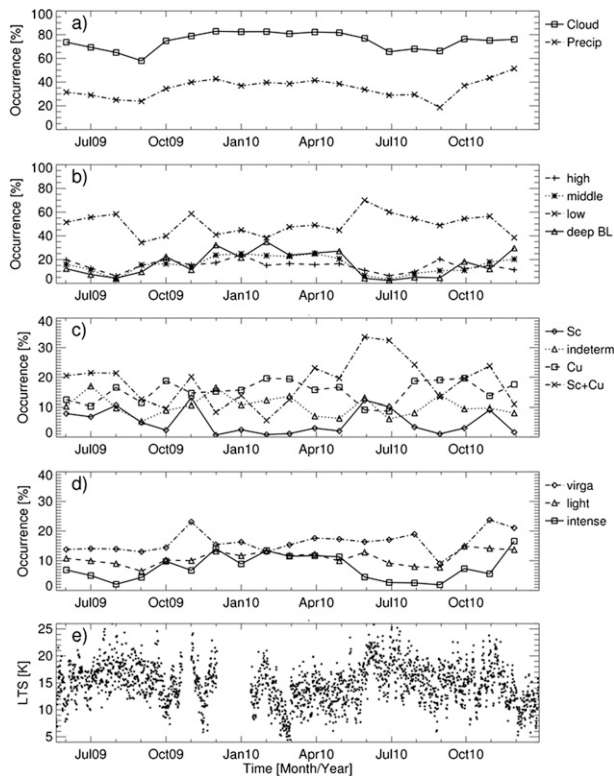


FIG. 3. Monthly statistics of (a) cloud and liquid precipitation coverage using the lidar–radar algorithm, (b) the four main cloud types, (c) low-level clouds, and (d) liquid precipitation types. Note that the September 2010 results come from only 8 days due to a radar downtime. Also note that the precipitation reported here relates to the first cloud layer only. (e) Time series of LTS as retrieved from the radiosondes launches.

seasonal cycle is observed with minimum (60%–70%) during the summer and early fall and maximum (80%) during the winter and spring season. Liquid precipitation is detected almost 50% of the time that we have hydrometeors in the atmospheric column and exhibits a similar weak seasonal cycle. A breakdown of the observed cloud occurrence into the four main cloud types (described in section 3a) is shown in Fig. 3b. Note that the sum of these cloud type occurrences is likely greater than (rather than equal to) the overall cloud occurrences shown in Fig. 3a since more than one cloud type can be present in the atmospheric column at the same time. Low-level clouds are the dominant observed cloud type, with 40%–60% occurrence maximizing in the summer and fall seasons. The seasonal cycle of low cloud occurrence anticorrelates with the observed seasonal cycle of all the other cloud types, which peaks during the winter and spring seasons (Fig. 3b), consistent with the presence of the subtropical high pressure system during the summer and fall seasons that favors MBL cloud

occurrence through the development of low-tropospheric stability and moisture trapping in the low levels. This system is strongest in summertime, when midlatitude storm tracks are at their most poleward, and with its center closer to the site (Hasanean 2004), explaining the seasonal cycle observed, as proposed by Norris and Klein (2000). A local minimum in the low cloud occurrence is noticeable in the early fall of 2009 (a corresponding 2010 event is unconfirmed owing to the radar failure in September 2010). This divergence could be a simple manifestation of interannual variability, experiencing more midlatitude systems than normal. A longer time series is needed to verify this feature.

Additional insights on the seasonal cycle of low-level clouds are provided through their breakdown into different subtypes (see Fig. 3c). Shallow cumulus clouds are the most frequently observed MBL cloud type with a monthly occurrence of 20% and weak month-to-month variability during the summer. Monthly increases in Sc + Cu coverage appear to compensate for decreases in the Cu cloud fraction. Indeed, this MBL cloud structure is also frequently observed, with maximum occurrences during the summer months. In fact, they follow a similar annual cycle as the single-layer stratocumulus clouds, which are the least observed MBL cloud type, especially during the winter and spring months. Nevertheless, the dataset is only long enough to derive an anecdotal seasonal climatology, as revealed by the differences between months in the first and second years. As for the indeterminate category, it has typical occurrences around 10% with small intraseasonal variability. Such low values probably come from the intermediate state of this type, acting as a transition between the other clouds based in the MBL (i.e., low and deep BL clouds).

The LTS has often been linked to the presence of low clouds. For instance, Zhang et al. (2010) provided coarse threshold values of LTS, less than 14 K and greater than 19 K, for small and large low-cloud fractions, respectively. These values correlate well with the cumulus and stratocumulus covers (see Fig. 3e). In fact, increases in LTS are usually associated with increases in stratocumulus coverage. Moreover, most values are close to or above the 14-K threshold, allowing cumulus clouds to form. This emphasizes the greater stability (mean of 17 K) found in the Azores, compared to the eastern equatorial Pacific (13 K; see Yin and Albrecht 2000).

Figure 3a demonstrates the propensity of marine clouds to produce precipitation. However, it often completely evaporates before reaching the surface, as illustrated by the separation into the three types considered (virga, light, and intense) in Fig. 3d. Intense precipitation occurs mostly during fall and winter, weakly following the presence of deep BL clouds, suggesting that it is primarily

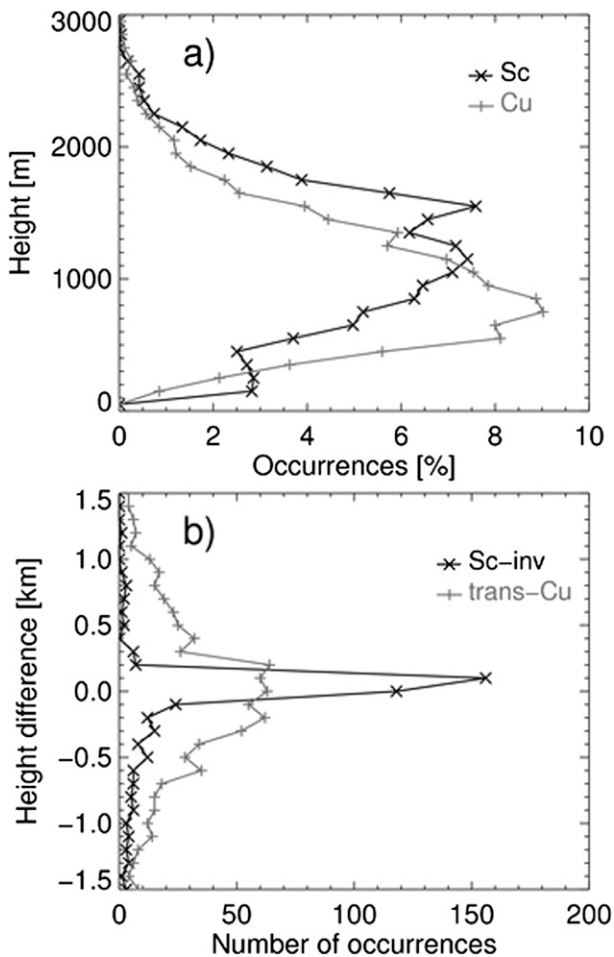


FIG. 4. (a) Distributions of the hourly cloud-base heights for the stratocumulus (black line) and cumulus (gray line) clouds. (b) Distributions of the distance between the transition layer and the cumulus hourly base (gray line) and between the stratocumulus hourly top and the inversion layer (black line).

associated with stronger and deeper systems. Other precipitation categories display no obvious annual variability.

b. Stratocumulus and cumulus cloud-base height statistics

According to Table 2, stratocumulus and cumulus clouds are separated based on their horizontal extent. Furthermore, their cloud-base height statistics are different and this improves the robustness of the radar-lidar-based classification algorithm. The distributions of their hourly averaged cloud-base heights are compared in Fig. 4a. Only hourly periods with a cloud fraction greater than 10% for the given type are included in the analysis. In addition, any hourly period with intense precipitation is also excluded to avoid possible contamination of the ceilometer cloud base. Although considerable variability in the cloud base occurrences of these two

cloud types is observed, a separation is clearly visible between the two distributions, with cumulus clouds forming lower than stratocumulus clouds. This is consistent with the frequently observed cumulus under stratocumulus MBL cloud structure in the Azores. Yet, some stratocumulus bases have been detected at very low altitudes (below 500 m, below most cumulus). Such low-based stratocumulus clouds have been sampled during ASTEX (de Roode and Duynkerke 1997); however, foglike conditions could have contaminated the statistics.

The hourly averaged stratocumulus cloud-top height and cumulus cloud-base height are compared with the MBL inversion base and the transition layer top, respectively (Fig. 4b). The MBL inversion base and transition layer top are estimated from the radiosondes. The cloud boundary heights used in the comparison with the radiosondes are 1-h averages centered on the sounding launch time. In addition, a minimum of 10% cloud fractional coverage is required and the absence of intense precipitation. The results are again in reasonable agreement with the expectations: both distributions are peaking near a zero difference, although the cumulus cloud base exhibits higher variability around the transition layer top. The broader distribution of cumulus cloud-base heights around the transition layer top height can be partially explained by their intermittent character and their role in maintaining the transition layer in the first place (Stevens 2007) and the difficulty in retrieving the hourly averaged cloud base, especially in shear conditions. Furthermore, part of the variability might be caused by the challenge of correctly detecting the transition layer in noisy soundings and from cumulus clouds linked to other clouds (i.e., breaking deep BL, stratocumulus, or indeterminate clouds).

The double-peak cloud-base height structure observed for the stratocumulus clouds is explained by their seasonal cycle (Fig. 5a). The lower peak (around 1100 m) results from summer cases, while the higher peak (around 1600 m) results from the transition periods (spring and fall, mainly May and September). The winter season did not experience much stratocumulus coverage (as noticed in Fig. 3c) and thus does not contribute much. This seasonal dependence could be linked to the dominant air mass, which in turn is influenced by the strength of the high pressure system. The agreement between the stratocumulus tops and the inversion base is still visible after averaging them monthly, except in winter when the stratocumulus clouds are less frequent (Fig. 5a). Interestingly, the averaged stratocumulus top is sometimes within the inversion layer. This agrees well with recent in situ observations (e.g., Carman et al. 2012), although the measurements have a great variability (not depicted

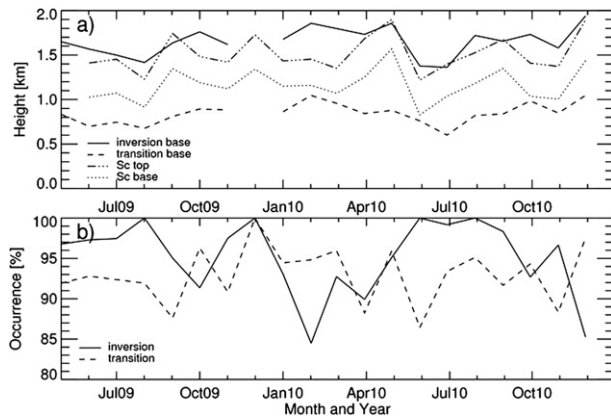


FIG. 5. Monthly statistics of (a) the transition and inversion layers base height and the stratocumulus clouds boundaries and (b) the occurrences of the inversion and transition layers, as a fraction of the number of soundings per month.

here) due to intraseasonal variations and various air mass intrusions. Another noticeable finding is the very frequent occurrence (higher than 80%) of inversion and transition layers in the MBL throughout the field campaign (Fig. 5b). The occurrence is based on the monthly fraction of soundings with inversion and/or transition layers. The persistence of transition layers indicates the lack of well-mixed conditions in the subcloud layer.

MBL VARIABILITY DURING SINGLE AND MULTILAYER CLOUD CONDITIONS

A detailed analysis of the MBL variability during stratocumulus and stratocumulus over cumulus conditions and their corresponding MBL thermodynamic structure is presented here. Since a vertical stratification of the MBL influences the development of these low clouds, the MBL thermodynamic structure is first investigated using the soundings directly, without classifying them by cloud type (see Fig. 5b). Inversion-topped MBLs were encountered by 95% of the soundings. Interestingly, the remaining 5% of the soundings, which are inversion free, occurred mostly in wintertime—the season when deep systems are more frequently observed. This also supports the strong influence of the nearby high pressure system, which would sustain the inversion cap through the divergence it creates. Similarly, 92% of the soundings presented a transition layer signature. However, this fraction is roughly the same for all studied months, showing no clear preference to any season. This is consistent with the constant coverage of cumulus clouds throughout the campaign, which help create and maintain this MBL structure (Stevens 2007).

The proportions of transition and inversion layers found in soundings are much larger than observed over the eastern equatorial Pacific (Yin and Albrecht 2000).

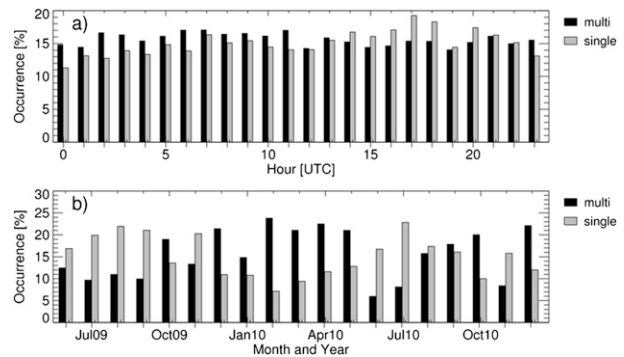


FIG. 6. (a) Daily and (b) annual cycles of hours characterized by single and multilayer clouds in the MBL (the gray and black bars, respectively). Each number of occurrences is normalized by the total number of hours with data within the considered hour in (a) or month in (b) to provide percentage values. Note that the local standard time in the Azores is UTC $- 1$ h.

It is reasonable to hypothesize that significantly strong mixing in the layer above the transition is required to support a clear temperature jump at its base. Radiative cooling associated with extensive clouds in the upper MBL may provide such mixing. In purely trade cumulus BL, this mixing is less efficient and the transition layer is less well defined. Interestingly, the transition layer height closely follows the inversion base height annually (see Fig. 5a), which further supports this hypothesis.

The MBL thermodynamic structure is also analyzed using its cloud structure. Every hour of the day, the time fraction of multilayer low clouds is recorded along with the standard deviation of the ceilometer first cloud base. If multilayer conditions exist for more than 10% of the hour and the cloud-base standard deviation is larger than 300 m (depicting broken clouds under a stratiform layer), then the hour is classified as multilayer cloud condition. On the other hand, if only a single cloud layer is detected within the hour and the cloud-base standard deviation is less than 100 m (ensuring a single level), then the hour is classified as single-layer cloud condition. Using the number of hours every month classified as single or multilayer cloud conditions, their diurnal and seasonal cycle can be estimated (Fig. 6). The observations suggest the presence of a weak diurnal cycle with increased single-layer occurrences during daytime and the opposite for multilayer conditions. Although this seems counterintuitive from a diurnal decoupling view, it is supported by the near-constant decoupled state of the MBL (see Fig. 5b), allowing cumulus to be omnipresent, while stratocumulus tend to fill in preferentially during nighttime. On the other hand, the MBL does show more multilayer cases in the wintertime and more single-layer clouds in the summertime, with associated transitions in the spring and fall seasons. This result is consistent with

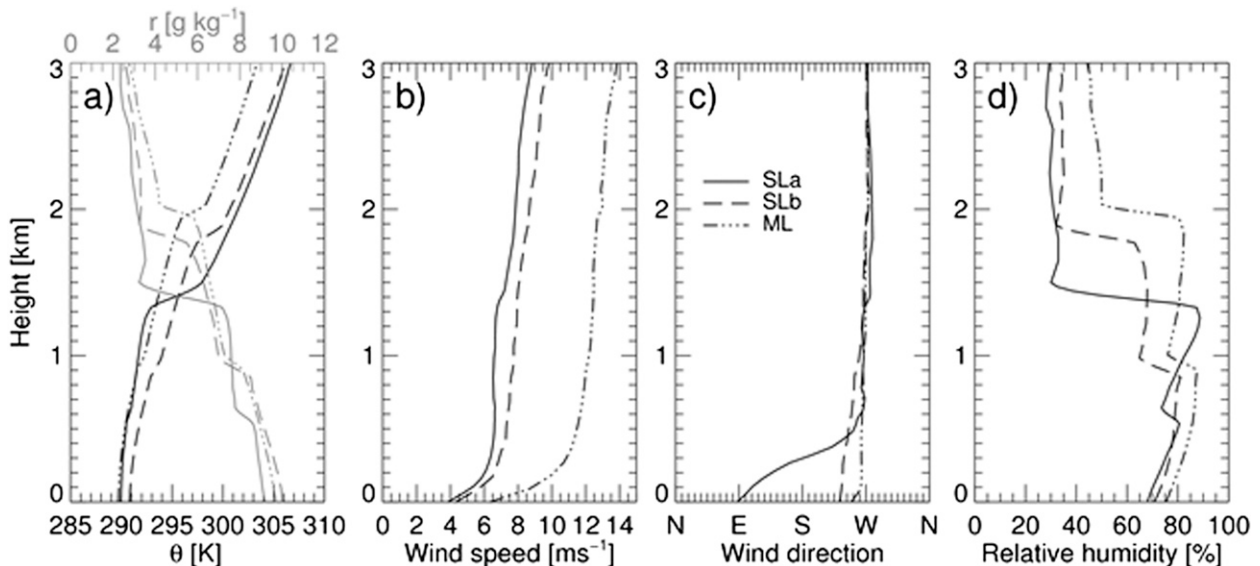


FIG. 7. Profiles of (a) potential temperature (black; bottom axis) and water vapor mixing ratio (gray, top axis), (b) wind speed, (c) wind direction, and (d) relative humidity composited over the cases with multiple BL clouds (dashed-dotted lines) and a single BL cloud at the inversion or transition level (solid and dashed lines, respectively), all presenting a transition layer.

a weaker high pressure system in winter, allowing for a weaker and higher (see Fig. 5a) inversion, providing more vertical extent to form multiple clouds.

The soundings collected within an hour of single and multilayer cloud conditions are further analyzed to identify the main feature of their corresponding thermodynamic structure in the MBL. Each sounding is first analyzed separately to detect the height of the inversion and transition layers (if present). The analysis indicated that the vast majority of the analyzed soundings that correspond to both single and multilayer cloud conditions show a transition layer (as seen in Fig. 5b). The soundings that did not have a detectable transition layer in the MBL were shallow (inversion height below 1 km), which might have prevented the complete formation of a transition layer. This concurs with previous studies (Albrecht et al. 1995; Wood and Bretherton 2004) suggesting that the atmospheric BL must be deeper than ~ 700 m to have a decoupled structure.

The single cloud layer soundings are separated in two subsets according to the thermodynamic layer linked to the cloud layer: the inversion (SLa) or the transition (SLb). A third category of soundings corresponds to multilayer cloud conditions (ML). Although the cloud type is not directly used in this classification, each group corresponds to a different MBL situation: stratocumulus (SLa), cumulus (SLb), and stratocumulus with cumulus underneath (ML). Using all soundings with a transition layer, composited profiles were obtained for each group following the layer-by-layer averaging method described in section 3b (see Fig. 7). The SLa cases have

a lower averaged inversion height, reminiscent of the difficulty to fully decouple shallow MBLs. They also have the strongest potential temperature and mixing ratio jumps through the inversion layer associated with the weakest jumps at the transition layer, supporting only the stratocumulus cloud. Comparatively, both layers show strong jumps for the SLb cases. A strong inversion in both types of single layer cases is consistent with their tendency to occur during summer, when the high pressure system is stronger.

The averaged profiles of potential temperature and mixing ratio exhibit a gradual transition from the stratocumulus (SLa) to stratocumulus with cumulus (ML) to cumulus (SLb) cloud regimes, supporting the usual picture of the transition from midlatitude to tropical MBL often experienced in the Azores (de Roode and Duynkerke 1997). The profiles with the lowest relative humidity correspond to cloud conditions associated with the transition layer only (SLb group), consistent with the broken nature of cumulus clouds. Multilayer cloud conditions show higher wind magnitudes on average. However, there is a great variability associated with the wind measurements, partly due to seasonal differences (not shown). The wind direction averaged profiles are very similar above the base of the transition layer; however, an easterly wind at the surface seems to be linked with single cloud layer detections near the inversion. Although not shown here, this change in direction in the SLa group happens in the summer, while fall cases are more unidirectional. Also, winter and spring single-layer cases tend to have a greater southern

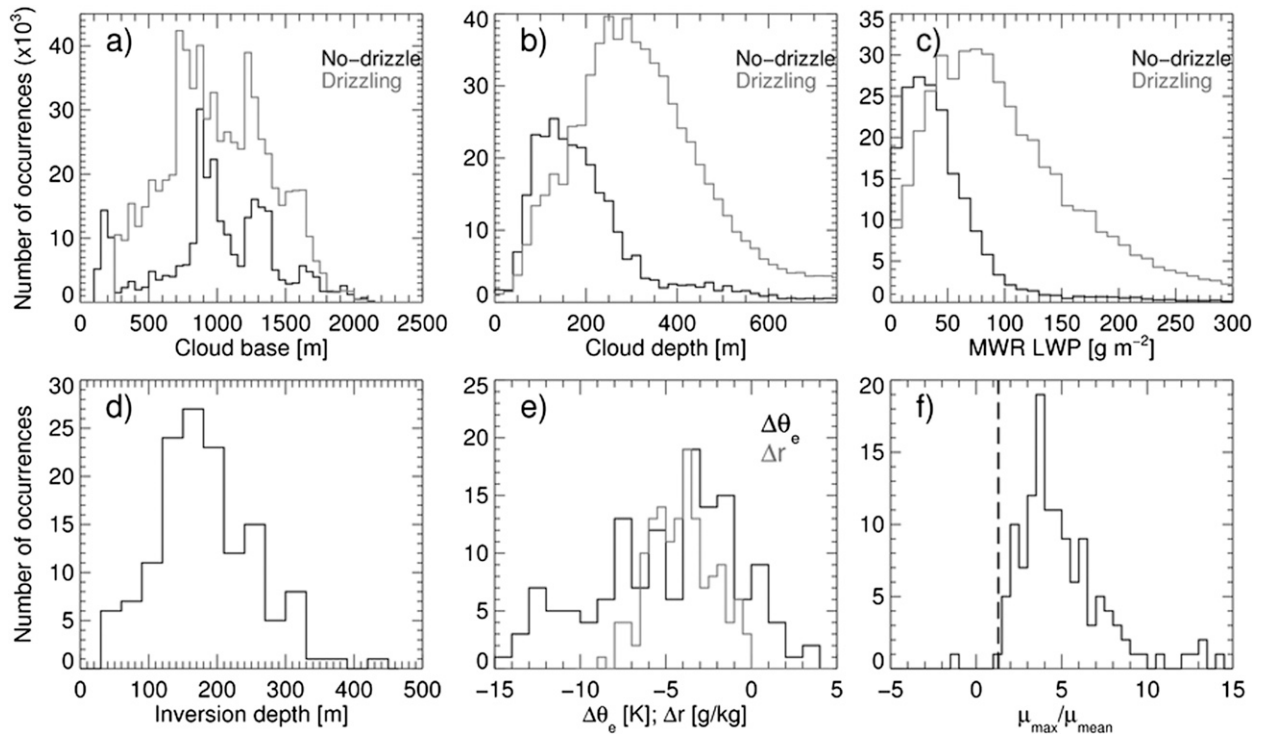


FIG. 8. Distribution of instantaneous (a) cloud base and (b) depth, (c) LWP, (d) inversion depth and (e) strengths, and (f) transition strength measured in the selected stratocumulus cases. In (a)–(c), measurements were divided according to the absence or presence of a drizzle shaft (the black and gray curves, respectively). In (e) the strength is reported in terms of equivalent potential temperature (black curve) and in terms of water vapor mixing ratio (gray curve). In (f) the vertical dashed line corresponds to the minimum value used to detect a transition layer (based on Yin and Albrecht 2000).

component. However, due to the wide range of variability in the data, more cases are needed to verify the existence (or lack of) of a preferred wind speed and direction (or synoptic situation) for each MBL structure through the seasons.

c. Stratocumulus clouds

1) MACROSCOPIC PROPERTIES AND THERMODYNAMIC STRUCTURE

Using the hours with single-layer stratocumulus conditions, 35 days when stratocumulus clouds persist through most of the day are selected for additional analysis. Most of the selected days occurred in early summer (June–July) or late fall (October–November). During the summer period, stratocumulus clouds have lower cloud-base heights compared to the late fall (causing the bimodal structure in Fig. 8a, as previously noticed in Figs. 4 and 5a using all stratocumulus clouds). A distinct difference in the distribution of cloud thickness is observed during drizzling (excluding intense precipitation) and nondrizzling conditions. The distribution of cloud thicknesses for periods with a drizzle shaft peaks around 250–300 m, while the distribution of cloud thicknesses

for periods without virga peaks at 150 m (Fig. 8b). On the contrary, there is no clear difference in the distributions of cloud bases using the same separation (see Fig. 8a). The peak below 200 m for the cases “without drizzle” comes mostly from periods when the ceilometer measurements are compromised by heavy precipitation, as they correspond to the tail of larger depths seen in Fig. 8b.

Another way to demonstrate the difference in cloud thickness during drizzling and nondrizzling periods is through their corresponding distributions of LWP (see Fig. 8c). Although small amounts of liquid water are possible in drizzling and nondrizzling stratocumulus clouds, LWP greater than 75–100 g m⁻² are sufficient to produce drizzling conditions. This result compares well with previous studies conducted in various stratocumulus decks (e.g., Wood 2005; Zuidema et al. 2005; Serpetzoglou et al. 2008; Kubar et al. 2009). Moreover, the nondrizzling distribution peaks around 30 g m⁻², which is near the theoretical accuracy of the deployed MWR. Also, as before, the tail of greater LWP visible for the nondrizzling profiles is associated with the deeper stratocumulus clouds with bases affected by precipitation.

The soundings recorded during the selected 35 days are used to describe the inversion and transition layer characteristics. As expected, all recorded soundings indicate the presence of an inversion layer near the stratocumulus cloud top. Owing to their small number (141) and the difficulty to properly define the associated drizzling character, no separation was performed. The depth of the inversion layer shows a strong peak just below 200 m (see Fig. 8d). This is much deeper than most observations (e.g., Carman et al. 2012) and simulations (e.g., Stevens et al. 1999). Nevertheless, this derived quantity is likely influenced by the smoothing of the data by the sounding software, as well as by wetting, which would have mainly caused an overestimate of the layer top (see Caldwell et al. 2005).

The full distributions of the jumps in equivalent potential temperature ($\Delta\theta_e$) and water vapor mixing ratio (Δr) are given in Fig. 8e. As observed in various stratocumulus studies, $\Delta\theta_e$ is often negative. Although this situation can still satisfy the stability criterion (Kuo and Schubert 1988; MacVean and Mason 1990) since Δr is usually also negative, most values fall within the range generally accepted for the criterion, and only a few soundings are clearly stable. Such persistence under unstable conditions has been observed in other studies (e.g., Faloon et al. 2005; Carman et al. 2012). Yamaguchi and Randall (2008) explain this behavior by the weakness of the feedback in stratocumulus.

Based on the methodology devised by Yin and Albrecht (2000) for the east Pacific (as described in section 3b), the presence of a transition layer was also diagnosed for most of the persisting stratocumulus soundings, as the threshold value was usually exceeded (see Fig. 8f). This suggests that the stratocumulus layer is decoupled from the surface.

2) DIURNAL CYCLE

Using the hourly derived statistics from the 35 selected days, a composite daily cycle is derived for the occurrence and boundaries of the stratocumulus clouds and their associated drizzle, using 3-h bins (Fig. 9). As expected, the cloud fraction is very high (>80%) throughout the day. The maximum values of cloud fraction are found during nighttime, with a gradual decrease of coverage occurring in the morning hours, followed by an increase after sunset, as in other marine decks (e.g., Ghate et al. 2009). The marine stratocumulus clouds observed in the Azores are usually precipitating (70% of the time), and the small decrease in cloud fractional coverage during daytime is also associated with a reduced drizzling fraction reaching ground. In fact, while virga is constantly detected in 45% of an average stratocumulus, light precipitation has a marked

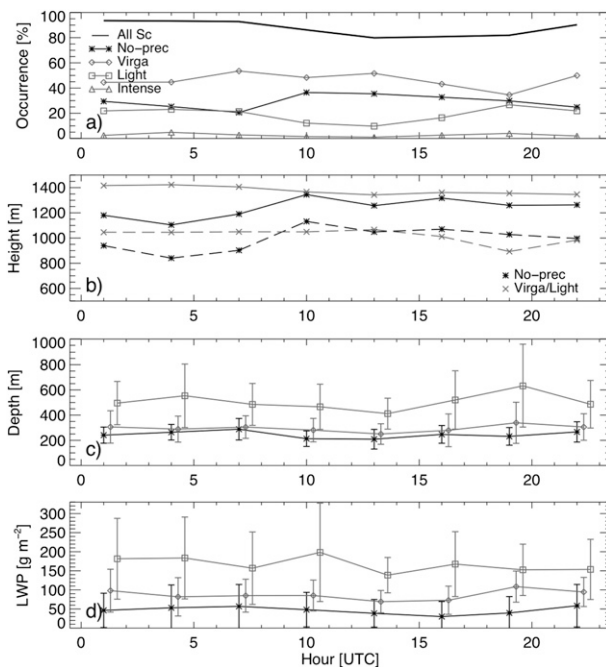


FIG. 9. Three-hourly statistics, composited from 35 days of persisting single-layer stratocumulus coverage, separated between periods without radar echoes below the cloud base and periods with various types of drizzle (virga, light, or intense): (a) fraction of the stratocumulus coverage, (b) cloud-base (dashed) and cloud-top (solid) heights, (c) cloud depth, and (d) LWP from the MWR. The average stratocumulus coverage is also included in (a) with the thick line. The error bars in (c),(d) represent the standard deviations.

decreased occurrence during the day. As for intense precipitation, it rarely occurs in a stratocumulus (less than 5%), and it is mostly around sunset and sunrise. Note that the panels of Fig. 9 show pseudo-daily cycles, as each value is the average weighted by the hourly fractions. As such, periods from various cases are mixed together, and the resulting cycle should be taken with a grain of salt, especially for the measurements affected by the seasons (e.g., boundaries heights).

Shallow MBLs are needed during nighttime to observe nondrizzling conditions, as indicated by the lower cloud boundaries, while the development of drizzle during daytime does not depend on the MBL depth (Fig. 9b). Light drizzle periods correspond to thicker cloud decks (cf. 450–550 m to 200–270 m) and higher LWP values (cf. 140–200 g m^{-2} to 30–60 g m^{-2}). Interestingly, virga periods have similar cloud depths (~ 300 m) as the nondrizzling periods but constantly show larger LWP values (70–100 g m^{-2}). Furthermore, only the LWP of virga periods have a distinctive daily cycle, with a pronounced increase near sunset. A similar cycle is observed in the cloud depth of the light drizzle periods, following its stratocumulus coverage (Figs. 9c,d). Note that the

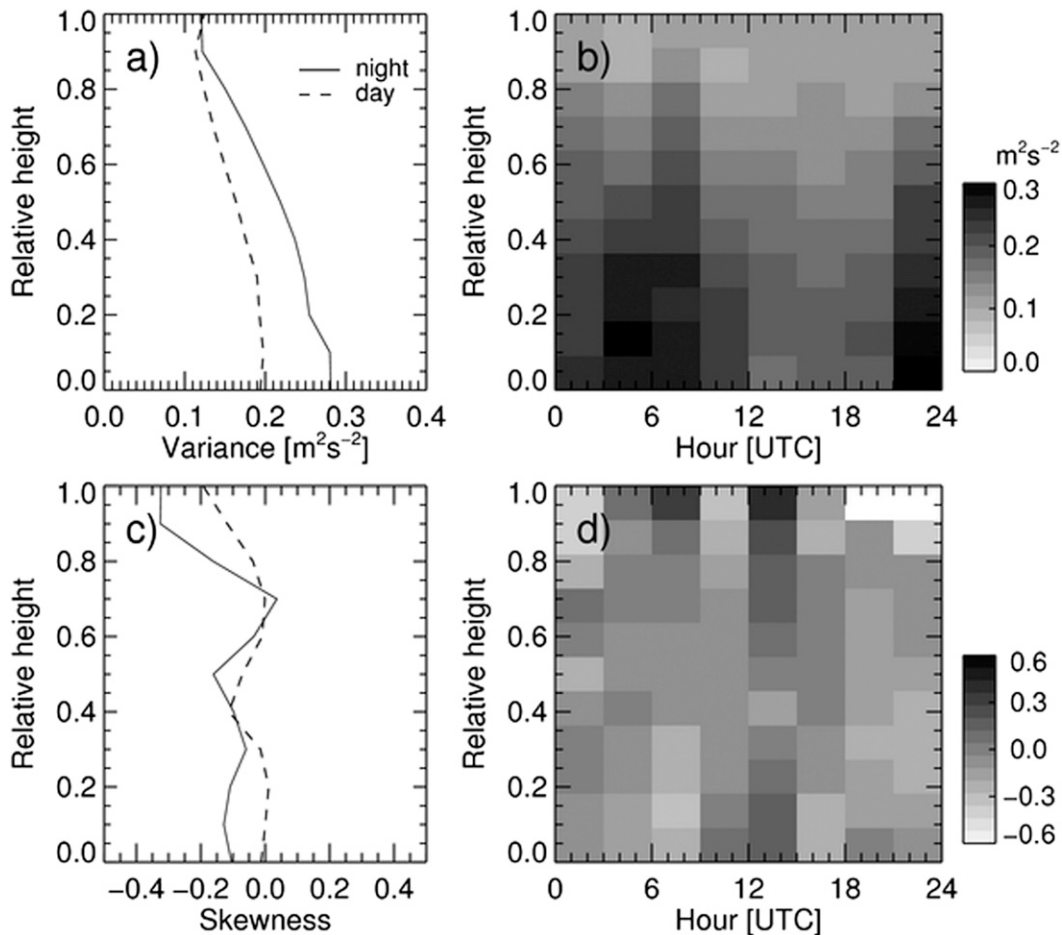


FIG. 10. Night (solid) and day (dashed) average profiles of the hourly estimated (a) variance and (c) skewness of the radar measured mean Doppler velocity and 3-hourly profiles of the (b) variance and (d) skewness of the radar measured mean Doppler velocity, composited over the selected periods of stratocumulus without drizzle under the cloud base. Note that the vertical axis represents the height above cloud base, in units of cloud depths, thus covering only the cloud layer.

variability between the cases remains important, creating some overlap.

3) VERTICAL AIR MOTION STATISTICS

Vertical air motions play an important role in the evolution of stratocumulus. Considering only the time periods without a drizzle shaft in the 35 selected cases, hourly vertical air motion statistics are derived (section 3c). Hours with less than 15% nondrizzling coverage are discarded from the following analysis. In the analysis, positive velocities indicate updrafts. Thus, negative skewness of the hourly distribution of vertical air motion indicates the presence of a few strong narrow downdrafts compensated by many weak broader updrafts. Daytime and nighttime composites of the vertical air motion statistics are constructed to highlight differences between day (1100–1700 UTC) and night

(2300–0500 UTC) time periods. Time periods close to local sunrise or sunset are discarded from this type of analysis to ensure a clear separation between the two periods.

The vertical air motion variance profiles peak at the cloud base (Fig. 10a). As noted in previous studies of the MBL (e.g., Nicholls 1989; Hignett 1991; Lothon et al. 2005; Guo et al. 2008; Ghate et al. 2010), it indicates a maximum of turbulent kinetic energy near the middle of the MBL since our measurements cover the top part of the MBL occupied with cloud. Higher variance is observed during nighttime, as observed by Hignett (1991), and is consistent with turbulence driven by cloud-top radiative cooling. This excess turbulent energy is responsible for the thickening of the stratocumulus deck, as well as its higher cloud fraction and stronger drizzle presence. The nighttime skewness

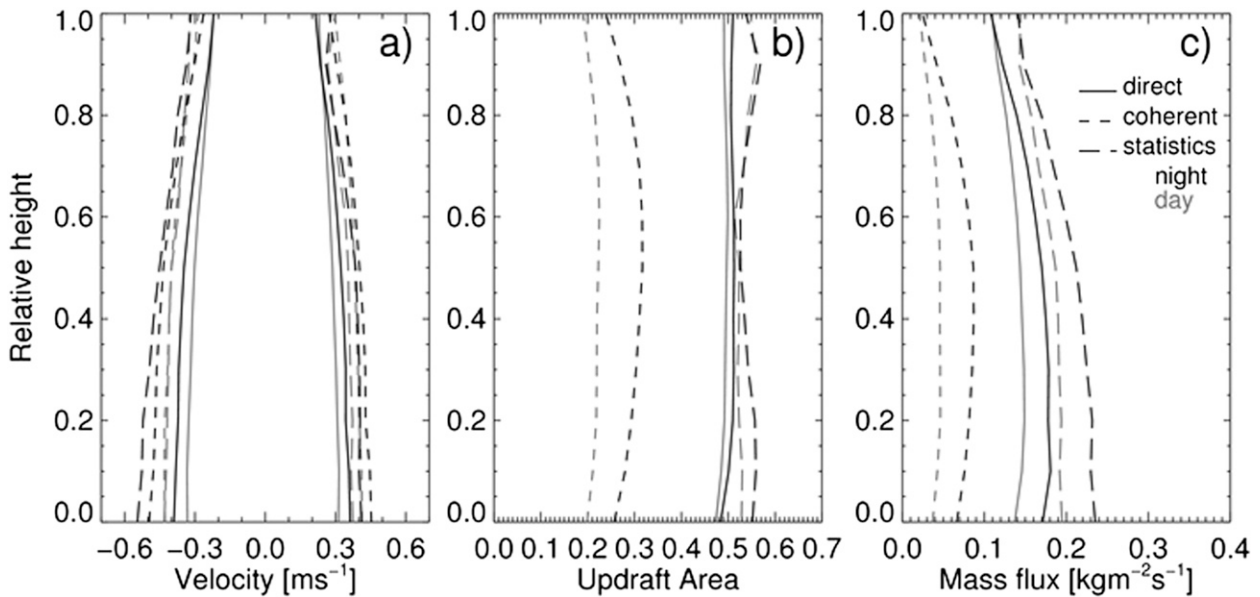


FIG. 11. Night (black) and day (gray) profiles of (a) updraft and downdraft velocities, (b) updraft area, and (c) mass flux associated with the updrafts, as obtained using three methods: direct sampling (solid lines), coherent structures only (short dashes), and the statistical method (long dashes).

profile of the vertical air motion is negative throughout the cloud layer (Fig. 10c). This is consistent with cloud-top radiative cooling as the driving mechanism and most nocturnal in situ observations (e.g., Kollias and Albrecht 2000; Guo et al. 2008). During daytime however, skewness values are closer to neutral in the lower two-thirds. Near the cloud top, both periods show a similar behavior, strong negative values, suggesting cloud-top-driven turbulence.

The diurnal evolution of the vertical air motion variance and skewness in the stratocumulus layer is shown in Figs. 10b,d using 3-h bins. The vertical air motion variance maximum is still clearly at night in the bottom half of the cloud. The periods exhibiting the highest variance values in the lower part of the cloud are 2100–2400 UTC and 0300–0900 UTC. Minimum vertical air motion variance in the lower part of the cloud is observed during the 1200–1800 UTC period. Close to the cloud top, the variance appears consistently low through the day. The diurnal cycle of the vertical air motion skewness better captures the role of cloud-top radiative cooling as a source of turbulence during nighttime. Positive values are also observed, but mostly in the top half during daytime, especially around noon when positive values appear to take over the whole cloud, consistent with surface-driven turbulence.

4) UPDRAFT MASS FLUX

The in-cloud vertical air motions support a significant portion of the turbulent transport of heat and moisture

in the cloud layer. The turbulence transport is often organized in temporally and spatially coherent updraft and downdraft structure. Here, the vertical air motion measurements are separated into nighttime and daytime periods and the analysis described in section 3c is applied to estimate the mean updraft and mean downdraft velocity profiles, the updraft area profile and the updraft mass flux profile. The resulting in-cloud profiles are shown in Fig. 11, using the three possible methods (direct, coherent, and statistical). First, note that the statistical technique gives generally the same profiles as the direct sampling, despite a small overestimate of the magnitudes, as found in LES models (Randall et al. 1992) and continental stratocumulus (Kollias and Albrecht 2000).

The mean amplitudes of velocity in updrafts and downdrafts are very similar. This is linked to the cloud separating into two halves (one going up, the other going down) on average throughout its depth, which compares well with continental stratocumulus clouds (e.g., Kollias and Albrecht 2000; Ghate et al. 2010) and other marine cases (e.g., Nicholls 1989; de Laat and Duynkerke 1998). However, coherent structures are responsible only for 40%–60% of the total mass flux. The contribution of coherent structures to the turbulent transport is maximized at night near the middle of the cloud. The mean velocity of coherent structures is also stronger, as expected. Nevertheless, their contribution to the mass flux is still limited, especially during daytime. As observed in the majority of stratocumulus decks, the mass flux

is greater during nighttime and in the bottom half of the cloud, when and where the turbulence is stronger. It is also linked to the mean velocities being maximized near the cloud base ($\sim 0.5 \text{ m s}^{-1}$), decreasing with height.

A similar analysis performed at the cloud base of cumulus gives comparable values, although the night and day results are closer. The main differences are stronger mean updraft and downdraft velocities and a weaker contribution from nighttime coherent structures. A more detailed analysis of the shallow cumulus cloud dynamics in the Azores can be found in Ghate et al. (2011).

5. Summary

The CAP-MBL campaign led to the collection of an extensive and well-documented ground-based dataset of MBL clouds. Here, the frequency of occurrence of different cloud and precipitation types along with their macroscopic properties (e.g., cloud boundaries) and MBL structure are presented. Several remote sensors are used to develop statistics of occurrence of various cloud and precipitation types. Clouds occur frequently throughout the 19-month period that was analyzed (June 2009–December 2010) with a maximum (80%) during the winter–spring months and a minimum (60%–65%) during the summer months. Precipitation occurrence is also very high (30%–40%), but precipitation only reaches the ground less than 15% of the time. Most intense precipitation events correlate well with the occurrence of non-MBL clouds linking them to mid-latitude cyclones during the winter and spring months.

A predominance of MBL clouds was observed all year long, while higher clouds show enhanced occurrences in winter. Moreover, cumulus clouds are present during all seasons, while stratocumulus clouds occur preferably during the transition periods. These two types often occur together, with each type being tied to a distinct thermodynamic layer (the cumulus to the transition layer and the stratocumulus to the inversion layer). The strength of the subtropical high pressure system influences the height (and presence) of the inversion, thus regulating the height of the stratocumulus layer, as well as the possibility to create two cloud layers in the MBL. In fact, on average, a stronger θ increase, a greater LTS value, and a lower inversion base tend to accompany a greater surface pressure in the Azores (a proxy for the strength of the subtropical anticyclone). In turn, although not shown here, a higher pressure also seems more favorable for a stratocumulus formation alone, while the cumulus clouds would form underneath at lower surface pressure.

Analysis of the sounding profiles demonstrates the near omnipresence of decoupling in the Azores MBL—a new finding that is only made possible by the long measurements made during the campaign. Cloud layers do not always reveal this decoupling, presenting only one layer in the observations. A two-part explanation can be hypothesized. First, a strong transition layer could prevent moisture from reaching the upper cloud layer. Second, a transition layer that is too weak might be unable to prevent the vertical development of cumulus clouds that would then fuse with the stratocumulus layer.

Thirty-five days characterized by the presence of persistent single-layer stratocumulus clouds were selected to gain further insights on their diurnal cycle, macroscopic properties (LWP and cloud boundaries), and dynamics. The minimum cloud coverage is observed in the afternoon. This is consistent with the findings of other studies using ground-based and satellite observations and models (e.g., Rozendaal et al. 1995; Abel et al. 2010). Although the fractions found here are greater (remaining above 80%), this is probably a bias due to the selection of persisting stratocumulus layers. Diurnal clearing is accompanied by a thinning of the cloud layer and a decrease in ground precipitation coverage and LWP. Again, this is consistent with other stratocumulus studies, such as those performed in the southeast Pacific (e.g., Wood et al. 2002; Abel et al. 2010). Furthermore, it was observed that stratocumulus is most likely to drizzle if the cloud depth exceeds 250 m and the LWP is above 60 g m^{-2} . Local maxima of ground precipitation coverage occur around sunrise and sunset.

We find that stratocumulus clouds are more turbulent during nighttime. Throughout the day, the turbulence maximized in the bottom half of the cloud, except around sunrise and after sunset when it extended through higher levels. Profiles of skewness from the velocity time series are consistent with cloud-top radiative cooling during nighttime and surface heating around noon, as reported in many other stratocumulus clouds (e.g., Kollias and Albrecht 2000). Mass flux is greater at night with the updrafts covering about half of the cloud, in accordance with observations in other decks and current theories (e.g., Nicholls 1989; de Laat and Duynkerke 1998; Kollias and Albrecht 2000). However, coherent updraft structures contribute 40%–60% of the total updraft mass flux. Higher contributions (70%–75%) have been observed in previous studies (e.g., Kollias and Albrecht 2000).

Various parts of the analysis were complicated, or even hindered, by the great variability observed between cases. Seasonal differences and air mass origin are likely to have a strong influence on this aspect. They

should be studied further to understand better their impacts. For the moment, it is difficult to know the aerosol source and content in each cloud, especially when the MBL has a decoupled structure.

REFERENCES

- Abel, S. J., D. N. Walters, and G. Allen, 2010: Evaluation of stratocumulus cloud prediction in the Met Office forecast model during VOCALS-REx. *Atmos. Chem. Phys.*, **10**, 541–10 559, doi:10.5194/acp-10-10541-2010.
- Albrecht, B. A., C. S. Bretherton, D. W. Johnson, W. H. Schubert, and A. S. Frisch, 1995: The Atlantic Stratocumulus Transition Experiment—ASTEX. *Bull. Amer. Meteor. Soc.*, **76**, 889–904.
- Augstein, E., H. Schmidt, and F. Ostapoff, 1974: The vertical structure of the atmospheric planetary boundary layer in undisturbed trade winds over the Atlantic Ocean. *Bound.-Layer Meteor.*, **6**, 129–150.
- Bony, S., and J.-L. Dufresne, 2005: Marine boundary layer clouds at the heart of tropical cloud feedback uncertainties in climate models. *Geophys. Res. Lett.*, **32**, L20806, doi:10.1029/2005GL023851.
- Bretherton, C. S., and Coauthors, 2004: The EPIC 2001 stratocumulus study. *Bull. Amer. Meteor. Soc.*, **85**, 967–977.
- Caldwell, P., C. S. Bretherton, and R. Wood, 2005: Mixed-layer budget analysis of the diurnal cycle of entrainment in southeast Pacific stratocumulus. *J. Atmos. Sci.*, **62**, 3775–3791.
- Carman, J. K., D. L. Rossiter, D. Khelif, H. H. Jonsson, I. C. Faloona, and P. Y. Chuang, 2012: Observational constraints on entrainment and the entrainment interface layer in stratocumulus. *Atmos. Chem. Phys. Discuss.*, **12**, 817–868, doi:10.5194/acpd-12-817-2012.
- Clothiaux, E. E., M. A. Miller, B. A. Albrecht, T. P. Ackerman, J. Verlinde, D. M. Babb, R. M. Peters, and W. J. Szyrmer, 1995: An evaluation of a 94-GHz radar for remote sensing of cloud properties. *J. Atmos. Oceanic Technol.*, **12**, 201–229.
- Comstock, K. K., R. Wood, S. E. Yuter, and C. S. Bretherton, 2004: Reflectivity and rain rate in and below drizzling stratocumulus. *Quart. J. Roy. Meteor. Soc.*, **130**, 2891–2918.
- de Laat, A. T. J., and P. Duynkerke, 1998: Analysis of ASTEX-stratocumulus observational data using a mass-flux approach. *Bound.-Layer Meteor.*, **86**, 63–87.
- de Roode, S. R., and P. G. Duynkerke, 1997: Observed Lagrangian transition of stratocumulus into cumulus during ASTEX: Mean state and turbulence structure. *J. Atmos. Sci.*, **54**, 2157–2173.
- de Szoeke, S. P., and S.-P. Xie, 2008: The tropical eastern Pacific seasonal cycle: Assessment of errors and mechanisms in IPCC AR4 coupled ocean–atmosphere general circulation models. *J. Climate*, **21**, 2573–2590.
- Faloona, I., and Coauthors, 2005: Observations of entrainment in eastern Pacific marine stratocumulus using three conserved scalars. *J. Atmos. Sci.*, **62**, 3268–3285.
- Garstang, M., and A. K. Betts, 1974: A review of the tropical boundary layer and cumulus convection: Structure, parameterization and modeling. *Bull. Amer. Meteor. Soc.*, **55**, 1195–1205.
- Ghate, V. P., B. A. Albrecht, C. W. Fairall, and R. A. Weller, 2009: Climatology of surface meteorology, surface fluxes, cloud fraction, and radiative forcing over the southeast Pacific from buoy observations. *J. Climate*, **22**, 5527–5540.
- , —, and P. Kollias, 2010: Vertical velocity structure of non-precipitating continental boundary layer stratocumulus clouds. *J. Geophys. Res.*, **115**, D13204, doi:10.1029/2009JD013091.
- , M. A. Miller, and L. DiPreto, 2011: Vertical velocity structure of marine boundary layer trade wind cumulus clouds. *J. Geophys. Res.*, **116**, D16206, doi:10.1029/2010JD015344.
- Guo, H., Y. Liu, P. H. Daum, G. I. Senum, and W. Tao, 2008: Characteristics of vertical velocity in marine stratocumulus: Comparison of large eddy simulations with observations. *Environ. Res. Lett.*, **3**, 045020, doi:10.1088/1748-9326/3/4/04520.
- Hasanean, H. M., 2004: Variability of the North Atlantic subtropical high and associations with tropical sea-surface temperature. *Int. J. Climatol.*, **24**, 945–957.
- Hignett, P., 1991: Observations of diurnal variation in a cloud-capped marine boundary layer. *J. Atmos. Sci.*, **48**, 1474–1482.
- Illingworth, A. J., and Coauthors, 2007: Cloudnet: Continuous evaluation of cloud profiles in seven operational models using ground-based observations. *Bull. Amer. Meteor. Soc.*, **88**, 883–898.
- Intrieri, J. M., M. D. Shupe, T. Uttal, and B. J. McCarty, 2002: An annual cycle of Arctic cloud characteristics observed by radar and lidar at SHEBA. *J. Geophys. Res.*, **107**, 8030, doi:10.1029/2000JC000423.
- Klein, S. A., and D. L. Hartmann, 1993: The seasonal cycle of low stratiform clouds. *J. Climate*, **6**, 1587–1606.
- Kollias, P., and B. Albrecht, 2000: The turbulence structure in a continental stratocumulus cloud from millimeter-wavelength radar observations. *J. Atmos. Sci.*, **57**, 2417–2434.
- , —, R. Lhermitte, and A. Savtchenko, 2001: Radar observations of updrafts, downdrafts, and turbulence in fair-weather cumuli. *J. Atmos. Sci.*, **58**, 1750–1766.
- , E. E. Clothiaux, M. A. Miller, E. P. Luke, K. L. Johnson, K. P. Moran, K. B. Widener, and B. A. Albrecht, 2007a: The Atmospheric Radiation Measurement Program cloud profiling radars: Second-generation sampling strategies, processing, and cloud data products. *J. Atmos. Oceanic Technol.*, **24**, 1199–1214.
- , G. Tselioudis, and B. A. Albrecht, 2007b: Cloud climatology at the Southern Great Plains and the layer structure, drizzle, and atmospheric modes of continental stratus. *J. Geophys. Res.*, **112**, D09116, doi:10.1029/2006JD007307.
- , J. Rémillard, E. Luke, and W. Szyrmer, 2011a: Cloud radar Doppler spectra in drizzling stratiform clouds: 1. Forward modeling and applications. *J. Geophys. Res.*, **116**, D13201, doi:10.1029/2010JD015237.
- , W. Szyrmer, J. Rémillard, and E. Luke, 2011b: Cloud radar Doppler spectra in drizzling stratiform clouds: 2. Observations and microphysical modeling of drizzle evolution. *J. Geophys. Res.*, **116**, D13203, doi:10.1029/2010JD015238.
- Kubar, T. L., D. L. Hartmann, and R. Wood, 2009: Understanding the importance of microphysics and macrophysics for warm rain in marine low clouds. Part I: Satellite observations. *J. Atmos. Sci.*, **66**, 2953–2972.
- Kuo, H.-C., and W. H. Schubert, 1988: Stability of cloud-topped boundary layers. *Quart. J. Roy. Meteor. Soc.*, **114**, 887–916.
- Lhermitte, R., 1990: Attenuation and scattering of millimeter wavelength radiation by clouds and precipitation. *J. Atmos. Oceanic Technol.*, **7**, 464–479.
- Liljegen, J. C., 1994: Two-channel microwave radiometer for observations of total column precipitable water vapor and cloud liquid water path. *Proc. Fifth Symp. on Global Change Studies*, Nashville, TN, Amer. Meteor. Soc., 262–269.
- Liu, Z., and Coauthors, 2009: The CALIPSO lidar cloud and aerosol discrimination: Version 2 algorithm and initial assessment of performance. *J. Atmos. Oceanic Technol.*, **26**, 1198–1213.
- Lothon, M., D. H. Lenschow, D. Leon, and G. Vali, 2005: Turbulence measurement in marine stratocumulus with Doppler radar. *Quart. J. Roy. Meteor. Soc.*, **131**, 2063–2080.

- Luke, E. P., P. Kollias, and M. D. Shupe, 2010: Detection of supercooled liquid in mixed-phase clouds using radar Doppler spectra. *J. Geophys. Res.*, **115**, D19201, doi:10.1029/2009JD012884.
- MacVean, M. K., and P. J. Mason, 1990: Cloud-top entrainment instability through small-scale mixing and its parameterization in numerical models. *J. Atmos. Sci.*, **47**, 1012–1030.
- Markowicz, K. M., P. J. Flatau, A. E. Kardas, J. Remiszewska, K. Stelmaszczyk, and L. Woeste, 2008: Ceilometer retrieval of the boundary layer vertical aerosol extinction structure. *J. Atmos. Oceanic Technol.*, **25**, 928–944.
- Mead, J. B., and K. B. Widener, 2005: W-band ARM cloud radar. Preprints, *32nd Int. Conf. on Radar Meteorology*, Albuquerque, NM, Amer. Meteor. Soc., P1R.3. [Available online at <http://ams.confex.com/ams/pdfpapers/95978.pdf>.]
- Münel, C., N. Eresmaa, J. Räsänen, and A. Karppinen, 2007: Retrieval of mixing height and dust concentration with lidar ceilometer. *Bound.-Layer Meteor.*, **124**, 117–128.
- Nicholls, S., 1989: The structure of radiatively driven convection in stratocumulus. *Quart. J. Roy. Meteor. Soc.*, **115**, 487–511.
- Norris, J. R., and S. A. Klein, 2000: Low cloud type over the ocean from surface observations. Part III: Relationship to vertical motion and the regional surface synoptic environment. *J. Climate*, **13**, 245–256.
- O'Connor, E. J., R. J. Hogan, and A. J. Illingworth, 2005: Retrieving stratocumulus drizzle parameters using Doppler radar and lidar. *J. Appl. Meteor.*, **44**, 14–27.
- Ramanathan, V., R. D. Cess, E. F. Harrison, P. Minnis, B. R. Barkstrom, E. Ahmad, and D. Hartmann, 1989: Cloud-radiative forcing and climate: Results from the Earth Radiation Budget Experiment. *Science*, **243**, 57–63.
- Randall, D. A., J. A. Coakley Jr., D. H. Lenschow, C. W. Fairall, and R. A. Kropfli, 1984: Outlook for research on subtropical marine stratiform clouds. *Bull. Amer. Meteor. Soc.*, **65**, 1290–1301.
- , Q. Shao, and C.-H. Moeng, 1992: A second-order bulk boundary-layer model. *J. Atmos. Sci.*, **49**, 1903–1923.
- Rozendaal, M. A., C. B. Leovy, and S. A. Klein, 1995: An observational study of diurnal variations of marine stratiform cloud. *J. Climate*, **8**, 1795–1809.
- Serpetzoglou, E., B. A. Albrecht, P. Kollias, and C. W. Fairall, 2008: Boundary layer, cloud, and drizzle variability in the southeast Pacific stratocumulus regime. *J. Climate*, **21**, 6191–6214.
- Stevens, B., 2007: On the growth of layers of nonprecipitating cumulus convection. *J. Atmos. Sci.*, **64**, 2916–2931.
- , C.-H. Moeng, and P. P. Sullivan, 1999: Large-eddy simulations of radiatively driven convection: Sensitivities to the representation of small scales. *J. Atmos. Sci.*, **56**, 3963–3984.
- , and Coauthors, 2003: Dynamics and Chemistry of Marine Stratocumulus—DYCOMS-II. *Bull. Amer. Meteor. Soc.*, **84**, 579–593.
- Ulaby, F. T., R. K. Moore, and A. K. Fung, 1981: *Microwave Remote Sensing Fundamentals and Radiometry*. Vol. 1, *Microwave Remote Sensing: Active and Passive*, Addison-Wesley, 456 pp.
- Wang, J., and W. B. Rossow, 1995: Determination of cloud vertical structure from upper-air observations. *J. Appl. Meteor.*, **34**, 2243–2258.
- Wood, R., 2005: Drizzle in stratiform boundary layer clouds. Part I: Vertical and horizontal structure. *J. Atmos. Sci.*, **62**, 3011–3033.
- , and C. S. Bretherton, 2004: Boundary layer depth, entrainment, and decoupling in the cloud-capped subtropical and tropical marine boundary layer. *J. Climate*, **17**, 3576–3588.
- , and —, 2006: On the relationship between stratiform low cloud cover and lower-tropospheric stability. *J. Climate*, **19**, 6425–6432.
- , —, and D. L. Hartmann, 2002: Diurnal cycle of liquid water path over the subtropical and tropical oceans. *Geophys. Res. Lett.*, **29**, 2092, doi:10.1029/2002GL015371.
- , and Coauthors, 2011: The VAMOS Ocean-Cloud-Atmosphere-Land Study Regional Experiment (VOCALS-REx): Goals, platforms, and field operations. *Atmos. Chem. Phys.*, **11**, 627–654, doi:10.5194/acp-11-627-2011.
- Yamaguchi, T., and D. A. Randall, 2008: Large-eddy simulation of evaporatively driven entrainment in cloud-topped mixed layers. *J. Atmos. Sci.*, **65**, 1481–1504.
- Yin, B., and B. A. Albrecht, 2000: Spatial variability of atmospheric boundary layer structure over the eastern equatorial Pacific. *J. Climate*, **13**, 1574–1592.
- Zhang, G. J., A. M. Vogelmann, M. P. Jensen, W. D. Collins, and E. P. Luke, 2010: Relating satellite-observed cloud properties from MODIS to meteorological conditions for marine boundary layer clouds. *J. Climate*, **23**, 1374–1391.
- Zuidema, P., E. R. Westwater, C. Fairall, and D. Hazen, 2005: Ship-based liquid water path estimates in marine stratocumulus. *J. Geophys. Res.*, **110**, D20206, doi:10.1029/2005JD005833.